Failure and Deformation Studies of Syndiotactic Polystyrene

MARY ANN JONES,[1] CRAIG J. CARRIERE,[2] MIKE T. DINEEN,[1] KAREN M. BALWINSKI[1]

[1] Designed Thermoplastics Research, 438 Building, The Dow Chemical Company, Midland, Michigan 48674

[2] Central Research and Development, 1702 Building, The Dow Chemical Company, Midland, Michigan 48674

Received 24 June 1996; accepted 14 August 1996

ABSTRACT: Syndiotactic polystyrene (sPS) is a chemically resistant, high-heat, semicrystalline polymer which is currently under development by The Dow Chemical Co. The research reported herein was undertaken to determine the critical fracture strength, i.e., the critical stress intensity factor, K_{1C}, and the fracture energy, G_{1C}, of sPS. The studies were aimed at developing a basic understanding of the failure mechanism and toughness of sPS. This work included investigations of the effect of molecular weight, as well as flow-induced anisotropy. Scanning electron microscopy (SEM) was used to aid in the determination of the failure mechanism. During failure testing, it was observed that sPS fails with a slow, controlled crack growth and ruptures with an almost nondetectable amount of yielding, as based on a tensile dilatometry investigation and a plane strain, biaxial yield experiment. The proposed failure mechanism, based on the scanning electron micrographs, is one of constrained crazing, followed by void coalescence with the spherulite nucleators acting as stress concentrators in the system. The damage appears to be greatly confined, with little initial cold-drawing of the spherulites. Addition of a nucleator reduces the K_{1C} values somewhat, as added nucleation sites proliferate the sites for stress concentration across the sample. © 1997 John Wiley & Sons, Inc. J Appl Polym Sci **64:** 673–681, 1997

Key words: syndiotactic polystyrene; fracture; deformation; void coalescence; tensile dilatometry

INTRODUCTION

Semicrystalline materials are beginning to find wider acceptance today in a number of engineering applications including electronic connectors, lighting, and automotive. As the use of these materials increases, it is of paramount importance to secure more quantitative information on their intrinsic toughness. This information is of use in predicting the utility of a material in a specific application, aiding in the modification of the material in areas such as glass reinforcement, and in finding optimum routes to toughen the materials. Experiments aimed at these issues have been reported for semicrystalline materials such as polypropylene and nylon,[1] poly(butylene terephthalate),[2–6] poly(vinylidene fluoride), nylon 6/6, and poly(acteal).[7]

Syndiotactic polystyrene (sPS) is a chemically resistant, high-heat, semicrystalline polymer which is currently under development by The Dow Chemical Co. Studies of the developed morphology of sPS under a number of different processing conditions have been reported[8–13] as well as modeling efforts.[14] However, a study of the failure and deformation processes of sPS has yet to be reported. This research reported herein was undertaken to determine the critical fracture strength, i.e., the critical stress intensity factor, K_{1C}, and the fracture energy, G_{1C}, of sPS. The studies were

Correspondence to: C. J. Carriere.

Table I Molecular Weight Characterization of sPS Materials

Sample History	aPS (kg/mol)	sPS Without Nucleator (kg/mol)	sPS Without Nucleator (kg/mol)	sPS Without Nucleator (kg/mol)	sPS With Nucleator (kg/mol)
Pellet $\bar{M}_w$	311	191	401	552	—
Final specimen $\bar{M}_w$	—	238	349	492	298

aimed at developing a basic understanding of the failure mechanism and toughness of sPS. This work included investigations of the effect of molecular weight as well as flow-induced anisotropy. Scanning electron microscopy (SEM) was used to aid in the determination of the failure mechanism. In addition, the results obtained on sPS are compared to those obtained for a high molecular weight atactic polystyrene (aPS) sample.

EXPERIMENTAL

Materials

Samples of sPS were obtained from The Dow Chemical Co., in the form of 5 × 5 × 0.125 in. injection-molded plaques, injection-molded Type I ASTM tensile bars, and injection-molded 5 × 0.5 × 0.060 in. strips. Samples of aPS were also obtained from The Dow Chemical Co. in the form of 6 × 6 × 0.125 in. compression-molded plaques. The aPS material was molded at 200°C with a 10 min heating time, 2 min cure time, and a 10 min cooling time. All the sPS samples examined in this work were injection-molded using a 150°C mold temperature, a barrel temperature of 310°C, an injection rate of 18 cm/s, and a cooling time of 60 s. The mold temperature was selected to minimize skin effects and achieve the maximum crystallinity (50%) throughout the sample.[15] One of the sPS materials was supplied containing an unspecified nucleating agent. All materials were used as received.

The molecular weights of the molded materials were measured using high-temperature size-exclusion chromotography (SEC) and are summarized in Table I. The SEC experiments were conducted at 135°C using 1,2,4 trichlorobenzene in a Waters 150C instrument.

Fabrication

Compact Tension Geometry

The compact tension specimens were machined from the delivered plaques. Specimens were machined from the plaques with the notch parallel as well as perpendicular to the direction of flow during the injection-molding process. The specimens were fabricated in accord with ASTM standard E399 with a thickness of 0.125 in. The average dimensions of the samples used in this study are illustrated in Figure 1.

Notching Technique

A notching apparatus was used to precrack each of the specimens. The apparatus was designed to hold the sample securely in a horizontal position while a utility blade is driven into the exact center of the machined notch using a hand-operated vise. Light pressure was applied until a sharp, subcritical crack ran out from the end of the utility blade. The sample was then examined under a light microscope to verify that the precrack did not bifurcate or exhibit bluntness.

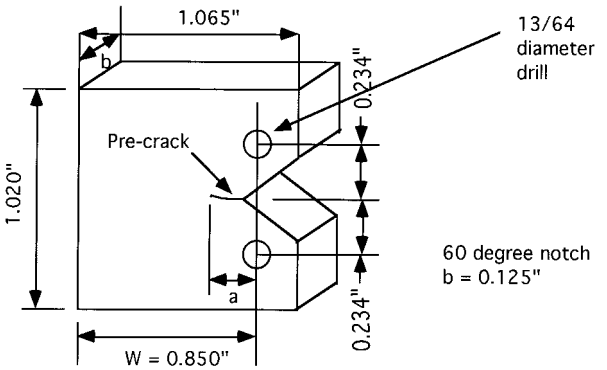

Figure 1 Schematic representation of the compact tension geometry used in the study.

Fracture Strength Investigations

The compact tension specimens were tested using a servohydraulic Instron 8500. The sample was subjected to a constant displacement rate of 0.02 in./min. The sample was placed under an initial load of 1 lb prior to testing. All the compact tension testing reported was obtained at 23°C and 50% relative humidity. The critical stress intensity factor, K_{1C}, was calculated using eqs. (1) and (2)[16]:

$$K_{1C} = \frac{P}{B\sqrt{W}} \times f\left(\frac{a}{W}\right) \tag{1}$$

where the function $f\left(\frac{a}{W}\right)$ is given by

$$f\left(\frac{a}{W}\right) = \frac{\left(2 + \frac{a}{W}\right)\left[0.886 + 4.64\left(\frac{a}{W}\right) - 13.32\left(\frac{a}{W}\right)^2 + 14.72\left(\frac{a}{W}\right)^3 - 5.6\left(\frac{a}{W}\right)^4\right]}{\left(1 - \frac{a}{W}\right)^{3/2}} \tag{2}$$

where P is the peak load; a, the length of the precrack; W, the sample width; and B, the sample thickness.

The fracture energy, G_{1C}, was calculated using[17]

$$G_{1C} = \frac{{K_{1C}}^2}{E} \tag{3}$$

where E is the Young's modulus as measured using a standard ultrasonic technique.[18,19]

Tensile Dilatometry Experiments

Poisson's ratios were obtained using an MTS servohydraulic system equipped with a biaxial strain gauge measuring axial and diametral strain. Glass cloth tape tabs were attached to the injection-molded sample bars at a 1 in. spacing and superglue was used to firmly attach the strain gauge to the tabs on the bar. All experiments were conducted at 23°C and 50% relative humidity at a constant displacement rate of 0.2 in./min. The experiment was extended to 5% axial strain or to specimen failure.

Biaxial, Plane Strain Yield Experiments

A biaxial, plane strain yield experiment was conducted to gain additional insight into the deformation mechanism. In this experiment, the sample was placed under a tensile stress and the compressive stress was varied to determine the point of yielding. Samples were run on equipment based on a design by Bowden and Jukes.[20] The apparatus is illustrated in Figure 2. The injection-molded sample bars were coated with a high viscosity, silicon-based grease which acts as a lubricant. The specimen bar was mounted in grips, with a weight of defined load attached. The weights were hung from a lever arm, allowing the loads to be amplified by 13.5 times the actual weight. A controlled pressure was applied at the center of the bar, across a 0.125 in. band. A micrometer was used to measure the change in thickness at this point of pressure, between 1 and 2 min time at the given loads. A change or creep rate of at least 0.003 in./min indicated yielding without rupture. The actual creep rate ranged from 0.003 to 0.025 in./min. If the sample broke before yielding, the data were discarded. The tensile load and compressive load were varied, generating a curve from zero tensile load to zero compressive load.

Fractography

Scanning electron microscopy (SEM) was used to investigate the surface of the fractured samples. Samples for SEM analysis were selected such that the specimen's K_{1C} value and load vs. displacement curve represented an average behavior for that material. The fracture surfaces were sputter-coated with gold palladium alloy and micrographs were taken on an ISI scanning electron microscope (Model ABT-55) at a 10° angle. The end of the precrack was marked with a razor blade to distinguish the precrack zone clearly from the fracture surface created during testing. Micro-

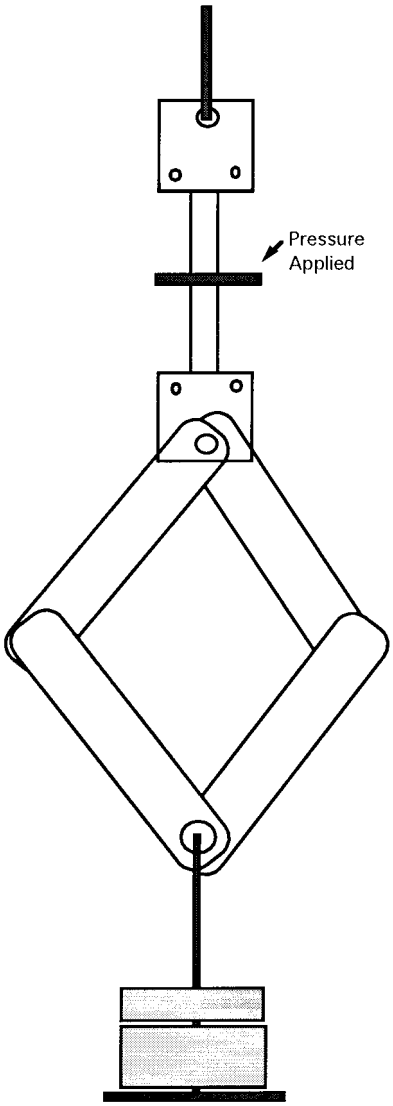

Figure 2 Schematic representation of the biaxial, plane strain yield apparatus.

graphs were taken at the core, sampling along differing points in the crack path, and also at the skin at the center point of the crack path.

RESULTS AND DISCUSSION

Critical Stress Intensity and Fracture Energy

Bulk fracture studies were run on neat sPS at varying molecular weights and compared with aPS. Samples were tested in both the machine and the transverse directions to determine the effect of orientation on the data. The values of K_{1C} obtained on the various sPS samples and aPS are summarized in Table II. sPS exhibited a lower value for K_{1C} than did the aPS sample, independent of the molecular weight of the sPS. Differences were detected in fracture strength as the molecular weight was varied, but clear trends were not observed. The direction of flow affected the aPS fracture strength but not that of neat sPS. Differences in the behavior of neat sPS and aPS during failure were observed. The aPS broke catastrophically when a peak load was reached but the sPS failed with a slow, controlled crack growth at much lower energy levels, as can be seen from the calculated G_{1C} values (Table II). The sPS sample containing the nucleator exhibited a moderate, but significant, drop in K_{1C} from that obtained on sPS without the nucleator.

Deformation Mode Analysis

Tensile dilatometry experiments were used to provide information on the increase in volume after yielding from void formation. The aPS sample crazed evenly across the entire bar and failed where expected, in the center region of the bar. The sPS did not display any visible damage zone and failed much closer to the gate end. The sPS and aPS materials performed very differently. The aPS sample crazed significantly, displaying craze bands on the sample, a drop in the Poisson's ratio, and a slight yielding in the stress–strain curve (Fig. 3). The sPS samples did not display any visual evidence of crazing before break, as based on the absence of any reduction in Poisson's ratio (Fig. 4). In addition, the sPS materials did not yield before rupture, based on the stress–strain curve.

Plane strain, biaxial yield testing provides another measurement of the ability of a material to yield. In general, a material will fail in a brittlelike fashion as its ability to yield is reduced and/or yielding occurs at higher stress levels (larger yield envelope).[20,21] The sPS material required a higher compressive stress to yield and broke immediately, as soon as any detectable yielding occurred. The aPS samples yielded at lower compressive stress and also to a much greater extent before sample failure (Fig. 5).

These two tests, when combined, define the general mode of deformation of these materials. Neither polymer displayed any sign of shear yielding in the tensile dilatometry test, as was expected. A polymer that shear yields would yield

Table II Summary of Measured Fracture Strength for aPS and sPS

Product	Orientation of Part	K_{1C} (MPa $\sqrt{m}$)	(SD)	G_{1C} (J/m^2)
Syndiotactic polystyrene	MD	1.20	(0.09)	350
$\bar{M}_w$ = 238 kg/mol	TD	1.15	(0.09)	
Syndiotactic polystyrene	MD	1.00	(0.16)	260
$\bar{M}_w$ = 298 kg/mol with nucleator				
Syndiotactic polystyrene	MD	1.62	(0.26)	420
$\bar{M}_w$ = 349 kg/mol	TD	1.55	(0.12)	
Syndiotactic polystyrene	MD	1.11	(0.09)	290
$\bar{M}_w$ = 492 kg/mol	TD	1.04	(0.05)	
Atactic polystyrene	MD	2.10	(0.44)	1800
$\bar{M}_w$ = 311 kg/mol	TD	2.72	(0.31)	
Atactic polystyrene	Compression-molded	2.42	(0.21)	1900
$\bar{M}_w$ = 311 kg/mol				

SD = standard deviation of K_{1c} data.
MD = machine direction, flow parallel to the direction of the crack.
TD = transverse direction, flow perpendicular to the direction of the crack.
Fracture energy, G_{1C}, was an average of machine and transverse data.
Fracture energy was calculated using the Young's modulus, as measured via a standard ultrasonic method.[17,18]

but display little decrease in the Poisson's ratio after yielding. The sPS samples exhibited more brittlelike failure when compared with aPS. This can be understood in the framework of evaluating the ability to craze and yield. The sPS appears to be inhibited in its ability to run long, stable crazes and to yield.

Fracture Surface Analysis

Scanning electron micrographs were taken at various places on the fracture surface and at varying

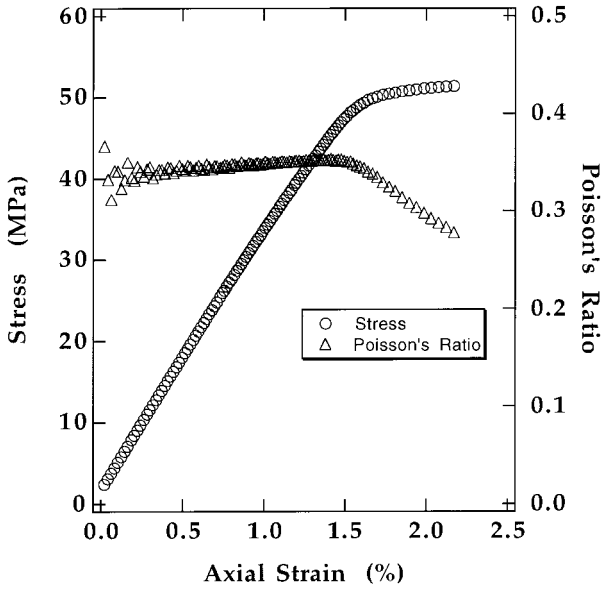

Figure 3 Example of the tensile dilatometry results for injection-molded aPS (311 kg/mol) at 23°C.

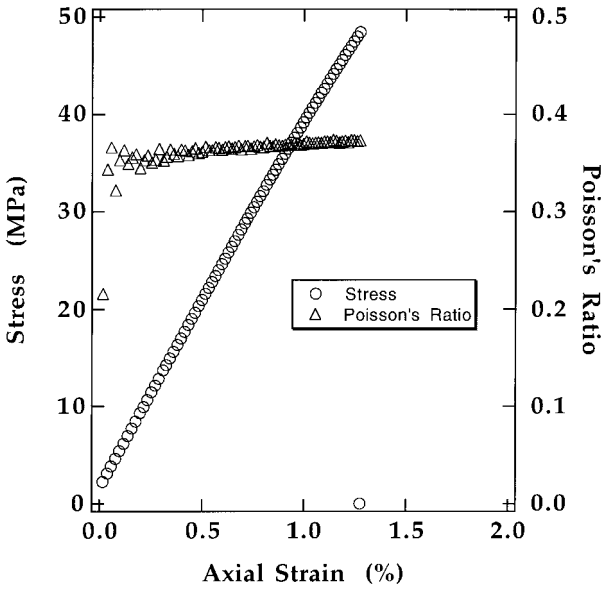

Figure 4 Example of the tensile dilatometry data for injection-molded sPS (349 kg/mol) at 23°C.

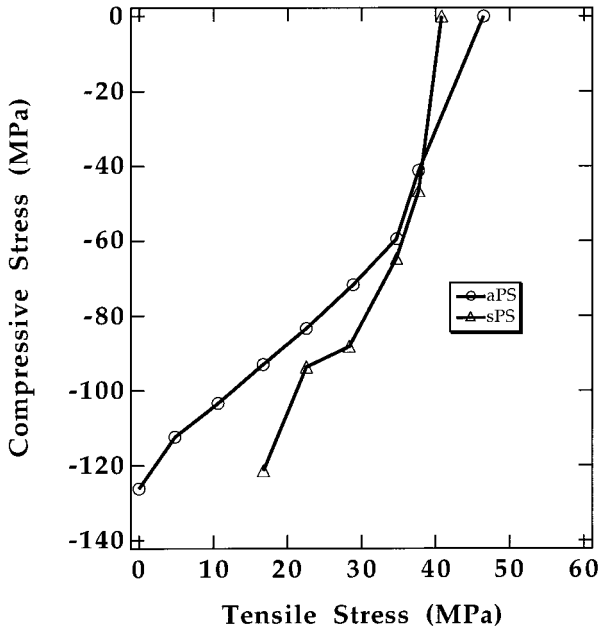

Figure 5 Example of biaxial, plane strain yield data for sPS (349 kg/mol) and aPS (311 kg/mol) at 23°C.

magnifications. The aPS sample is typical of a brittle thermoplastic, containing most of the fracture surface features seen with a catastrophic break. A smooth, flat mirror zone is seen where the sharp precrack was placed [Fig. 6(a)]. It appears featureless and is usually associated with slow crack growth near the fracture origin. A very small hazy region is observed adjacent to the precrack edge [Fig. 6(b)]. This is typically associated with crack acceleration prior to rapid crack growth. Hackle lines radiate out from the fracture origin, indicating high crack velocity and rapid changes in the stress field and fracture paths [Fig. 6(a)–(d)]. The Hackle lines are consistent with the catastrophic failure observed. Wallner lines are the faint striations resembling a periodic, wavelike pattern [Fig. 6(a) and (c)]. They reflect the changes in the stress wave velocity as the crack front progresses during crack propagation. "Stringers" were also observed at high magnifications [Fig. 6(d)]. They extend between the Hackle lines and may indicate some polymer drawing as the crack progressed. Drawn material can be observed even in a brittle material, due to the significant level of localized heating that occurs in the fracture process.

The sPS materials fracture in a very different manner than does aPS. A honeycomb-type pattern of damage can be observed on the failure surface. The size of the pattern is consistent with the approximate spherulite size in sPS without the nucleator. The current proposed theory on the failure mechanism assumes that the spherulite nucleators, as well as other contaminants, act as stress concentrators in the system. It is assumed that, initially, crazes are formed between crystalline lamellae. The damage areas radiate out and void coalescence is observed [Fig. 7(a)]. A rough correspondence between the average spherulite size and the average void size is often apparent. Damage zones initiating at the site of nucleation would tend to meet approximately at the spherulitic interfaces. The semicrystalline nature of sPS inhibits the ability of the sample to run long crazes greater than a few 100 Å and to yield. The whitened pattern is actually drawn polymer, as can be seen in another SEM taken at a 30° angle [Fig. 7(b)]. This theory is consistent with the low fracture strength measured and with the lack of crazing and yielding evident in the tensile dilatometry test and the plane strain, biaxial yield test.

The assumptions above include the hypothesis that little deformation is going on within the spherulites near the fracture zone during early stages of deformation. Most ductile semicrystalline polymers are thought to fail in a manner that involves a significant amount of spherulitic deformation and damage. Three stages of plastic deformation are cited typically in the plastic deformation process of crystalline materials.[22] The first stage is plastic deformation of the spherulitic structure. Plastic deformation occurs through lamella slip followed by the rotation of the lamella toward a parallel orientation with the tensile stress (deformation of the spherulite but not the lamellae). The second stage is the transformation of the spherulitic structure into a fibrous structure. The lamellae fracture and form microfibrils, changing from stacks of parallel lamellae into bundles of aligned, densely packed microfibrils. Type 2 crazes form, perpendicular to the principal stress and bridged by the fibrils. Type 2 crazes differ from the type 1 crazes occurring in amorphous polymers, growing in the stress but not in the perpendicular direction. The crazing is terminated when all of the spherulitic material has been transformed into a fibrous structure and involves a large portion of the material, as opposed to the localized type 1 crazes in amorphous polymers. The third stage involves the plastic deformation of the fibrous structure. Fibrils slide on each other and deform through a shear displace-

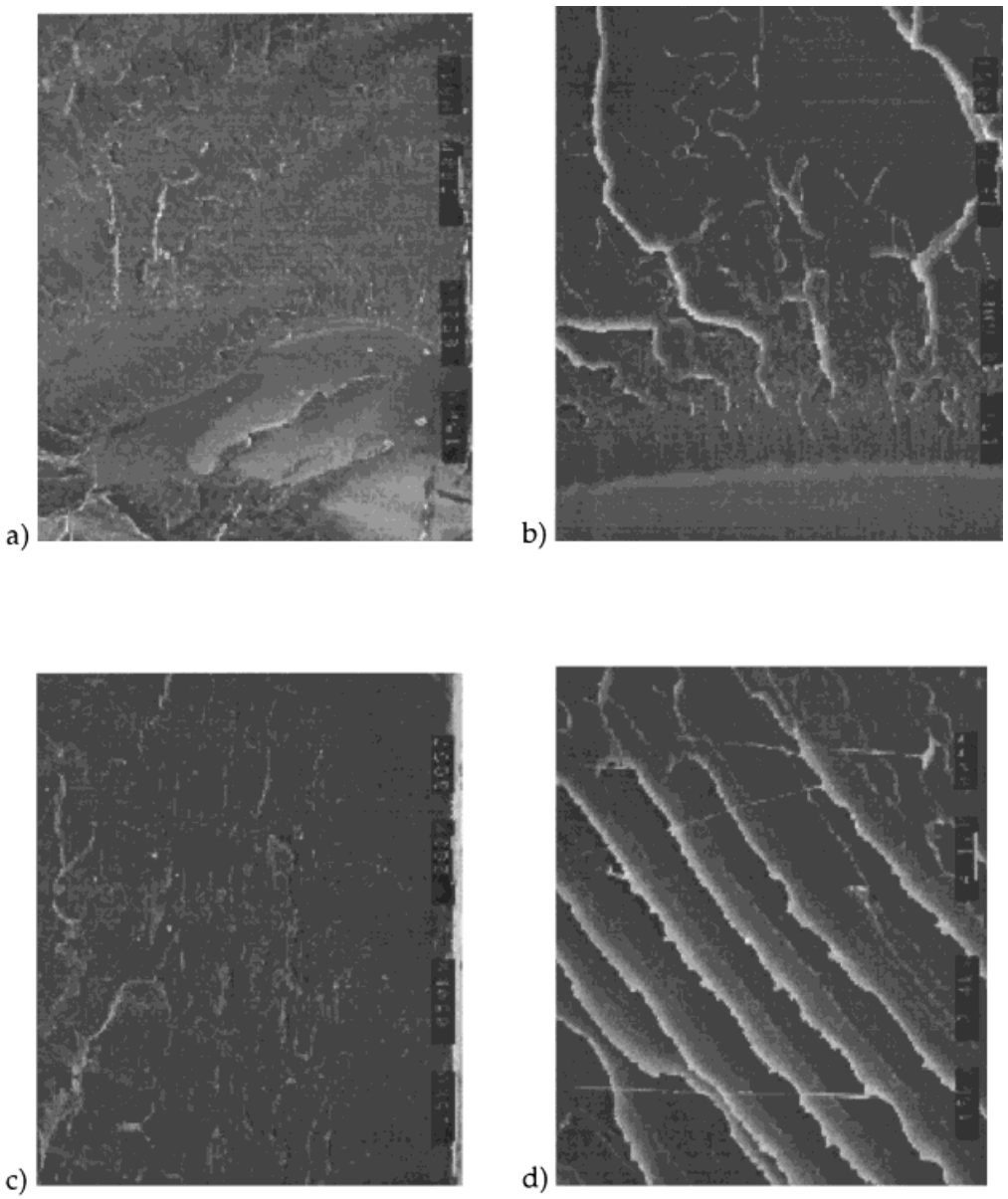

Figure 6 SEM micrographs of MD aPS fracture surfaces taken at (a) the fracture beginning at 50×, (b) the fracture beginning at 600×, (c) the fracture middle at 50×, and (d) the fracture beginning at 2500×. All micrographs were taken using a 10° tilt angle.

ment of the microfibrils. This leads to void formation and eventual failure.[22]

These stages of deformation were developed primarily through the study of polyolefins and other low T_g crystalline polymers. A very different fracture mechanism can sometimes occur if these same polymers are tested at very low temperatures. Very little microfibril formation occurs. sPS is approximately 80° below its T_g, when tested at room temperature. This would be comparable to the very low temperature testing of polyolefins, as one considers the constraint of chain mobility. Low-temperature testing is a technique often used to study the spherulitic structure of a polymer through electron microscopy.[22] The scanning electron micrographs of neat sPS are consistent with the idea that void coalescence is occurring at the spherulitic boundaries.

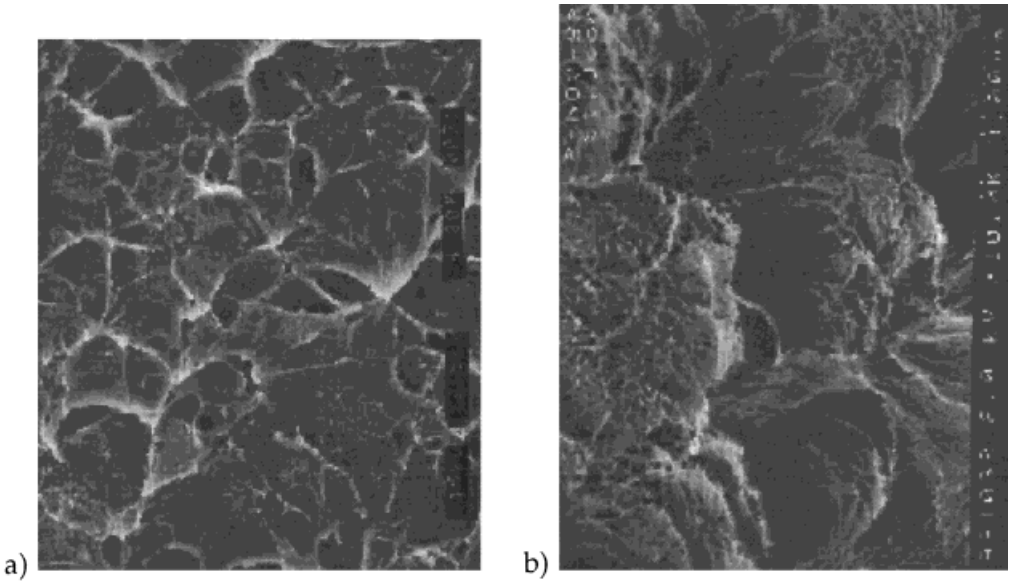

Figure 7 SEM micrographs of MD sPS fracture surfaces taken at (a) the end of the fracture at 2500× and a tilt angle of 10° and (b) the end of the fracture at 10,000× and a tilt angle of 30°. The sPS samples did not contain any nucleator.

The fracture surface for the sPS material containing the nucleator is illustrated in Figure 8. A smaller damage pattern with more void sites is evident in the micrograph, indicative of the smaller spherulitic size expected from the addition of a nucleator. If the nucleated sites are acting as stress concentrators in the material, this may be the cause of the decreased value of K_{1C} measured.

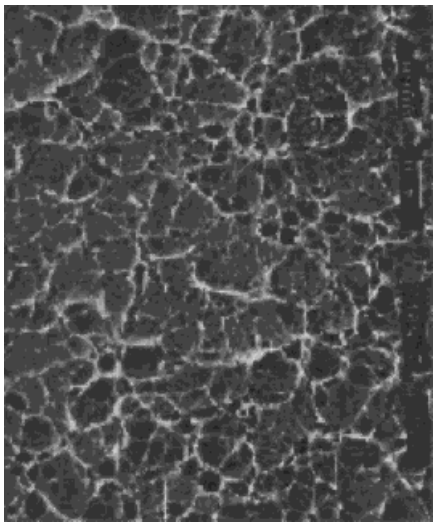

Figure 8 SEM micrograph of the fracture surface of MD sPS specimens containing nucleator.

CONCLUSIONS

The sPS materials investigated in this work exhibited markedly different failure behavior than that of a high molecular weight aPS sample. Both K_{1C} and G_{1C} values indicate that sPS fails in a more brittlelike fashion than does the high molecular weight aPS sample. The materials investigated failed in a different manner, with aPS breaking catastrophically and sPS failing with a slow, controlled crack growth. aPS crazes significantly and yields, whereas the sPS ruptures with an almost nondetectable amount of yielding, as based on a tensile dilatometry investigation and a plane strain, biaxial yield experiment. The proposed failure mechanism, based on the scanning electron micrographs, is one of constrained crazing, followed by void coalescence with the spherulite nucleators acting as stress concentrators in the system. The damage appears to be greatly confined, with little initial cold-drawing of the spherulites. Addition of nucleator reduces the K_{1C} values somewhat, as added nucleation sites proliferate the sites for stress concentration across the sample.

REFERENCES

1. G. P. Marshall, L. H. Coutts, and J. G. Williams, *J. Mater. Sci.,* **9,** 1409 (1974).

2. S. Y. Hobbs and R. C. Bopp, *Polymer,* **21,** 559 (1980).
3. J. E. Callear and J. B. Shortall, *J. Mater. Sci.,* **12,** 141 (1977).
4. B. Möginger, C. Lutz, A. Polsak, and U. Müller, *Colloid Polym. Sci.,* **269,** 535 (1991).
5. C. R. Joe and B. H. Kim, *J. Mater. Sci.,* **25,** 1991 (1990).
6. S. Y. Hobbs and C. F. Pratt, *J. Appl. Polym. Sci.,* **19,** 1701 (1975).
7. P. E. Bretz, R. W. Hertzberg, and J. A. Manson, *Polymer,* **22,** 1272 (1981).
8. F. de Candia, A. Ruvolo Filho, and V. Vittoria, *Colloid Polym. Sci.,* **269,** 650 (1991).
9. F. de Candia, R. Russo, and V. Vittoria, *J. Polym. Sci. Polym. Lett.,* **28,** 203 (1990).
10. F. de Candia, G. Romano, R. Russo, and V. Vittoria, *Colloid Polym. Sci.,* **268,** 720 (1990).
11. F. de Candia, M. Carotenuto, L. Guadagno, and V. Vittoria, *Macromolecules,* **25,** 6361 (1992).
12. N. M. Reynolds and S. L. Hsu, *Macromolecules,* **23,** 3463 (1990).
13. D. H. Krzystowczyk, X. Niu, R. D. Wesson, and J. R. Collier, *Polym. Bull.,* **33,** 109 (1994).
14. Z. Sun, R. J. Morgan, and D. N. Morris, *Polymer,* **33,** 725 (1992).
15. D. H. Bank, T. E. Wessel, and J. J. Kolb, in *Society of Automotive Engineers International Congress,* March 1993, p. 96.
16. H. L. Ewalds and R. J. H. Wanhill, *Fracture Mechanics,* Edward Arnold, London, 1991, p. 51.
17. H. L. Ewalds and R. J. H. Wanhill, *Fracture Mechanics,* Edward Arnold, London, 1991, p. 20.
18. J. R. Frederick, *Ultrasonic Engineering,* Wiley, New York, 1965.
19. G. L. Gooberman, *Ultrasonics Theory and Application,* Hart, New York, 1968.
20. P. B. Bowden and J. A. Jukes, *J. Mater. Sci.,* **3,** 183 (1968).
21. R. A. Bubeck, S. E. Bales, and H.-D. Lee, *Polym. Eng. Sci.,* **24,** 1142 (1984).
22. A. Peterlin, *Polymeric Materials, Relationships Between Structure and Mechanical Behavior,* American Society for Metals, 1973.